PLANAR POLARIZATION OF CILIA IN THE ZEBRAFISH FLOOR PLATE INVOLVES Par3-MEDIATED POSTERIOR LOCALIZATION OF HIGHLY MOTILE BASAL BODIES.

Antoine Donati[1], Sylvie Schneider-Maunoury[1*] and Christine Vesque[1*]

[1] Sorbonne Université, CNRS UMR7622, INSERM U1156, Institut de Biologie Paris Seine (IBPS) - Developmental Biology Unit, 75005, Paris, France

*co-senior authors, co-corresponding authors.

Keywords: planar cell polarity, cilium, basal body, zebrafish floor plate, Par3, Vangl2.

ABSTRACT

To produce a directional flow, ciliated epithelia display a uniform orientation of ciliary beating. Oriented beating requires planar cell polarity (PCP), which leads to planar orientation and asymmetric positioning of the ciliary basal body (BB) along the polarity axis. We took advantage of the polarized mono-ciliated epithelium of the embryonic zebrafish floor plate (FP) to investigate by live-imaging the dynamics and mechanisms of BB polarization. We showed that BBs, although bearing a cilium, were highly motile along the polarity axis, contacting either the anterior or posterior membranes, exclusively at the level of apical junctions positive for Par3. Par3 was posteriorly enriched before BB posterior positioning and FP polarization was disrupted upon Par3 overexpression. In the PCP mutant *Vangl2*, BBs showed poorly oriented movements correlated with Par3 mislocalization. Our data lead us to propose a conserved function for Par3 in controlling BB asymmetric positioning downstream of the PCP pathway.

INTRODUCTION

Cilia are conserved microtubule-based organelles with sensory and motile functions. Motile cilia generate forces sufficient to propel whole organisms or bodily fluids within cavities in animals: in respiratory airways to clear the mucus, in the oviduct to move gametes, in the embryonic laterality organ to establish left-right asymmetry, and in the central nervous system to propel the nutrient-rich cerebrospinal fluid (Wallingford 2010; Meunier & Azimzadeh, 2016). In order to generate a directional flow, ciliated epithelia display a uniform orientation of ciliary beating, which is a form of planar cell polarity (PCP). Oriented beating of a cilium usually involves two PCP processes: the off-centering of the cilium basal body (translational polarity, in monociliated epithelia and ependymal cells) and the orientation of its beating relative to the main tissue axis (rotational polarity) (Wallingford 2010).

In many vertebrate ciliated tissues such as the mouse cochlea and ependyma, the laterality organ of mouse and zebrafish, the Xenopus larval skin and the zebrafish floor plate, cilium polarity requires the PCP pathway. In these tissues, PCP proteins such as Van Gogh like 2 (Vangl2), Frizzled (Fz3/6), Cadherin EGF LAG seven-pass G-type receptors (Celsr1-3) and Dishevelled (Dvl1-3), localize asymmetrically in ciliated epithelia, and are required for proper cilia/BB positioning (Montcouquiol et al., 2003, Mitchell et al., 2009, Borovina et al., 2010, Mirzadeh et al., 2010, Song et al 2010, Boutin et al., 2012). Outside the PCP pathway, the cellular and molecular mechanisms of BB positioning remain poorly understood. Non-muscle myosin II is required for ependymal translational polarity in murine ependymal multiciliated cells (Hirota et al., 2010) and the murine Myosin Id mutant exhibit defects in both translational and rotational polarity in these cells (Hegan et al., 2015). Translational polarity has been shown to require Rac1 in monociliated cells of the mouse node and cochlea (Hashimoto et al., 2010; Grimsley-Myers et al., 2009) and G protein signalling in cochlear hair cells (Ezan et al., 2013; Tarchini et al., 2013). Ciliary proteins themselves have been involved in planar polarization of cilia in several contexts (Ross et al., 2005; Jones et al., 2008; Mirzadeh et al., 2010; Mahuzier et al., 2012; Ohata et al., 2015). However, the relationships between these different actors and how they impact basal body movement is unclear.

Understanding the mechanisms of cilium polarization would highly benefit from a dynamic analysis of BB movements. A major drawback is the difficulty to follow the dynamics of BB polarization *in vivo* in whole embryos, or to reproduce PCP and cilium polarization *in vitro* in cultured cells. So far, live imaging of cilium polarization has been performed only in cochlear explants where only confined Brownian motion of centrioles was observed (Lepelletier et al., 2013) and in the mouse node (Hashimoto 2010) and ependyma (Hirota 2010) with very limited temporal resolution. In this paper, in order to get a better understanding of the mechanisms leading to BB off-centering in epithelia, we have used the zebrafish embryonic floor-plate (FP) as a convenient system to investigate the dynamics of the polarization process in live embryos. The FP is a simple mono-ciliated epithelium whose posterior-positioned motile cilia allow circulation of the embryonic CSF in an anterior to posterior fashion.

Our results show that planar polarization of BBs and their associated cilia is progressive during somitogenesis and is accompanied by a change in the behavior of the BBs, which are highly motile at early stages and tend to spend an increasing amount of time in contact with the posterior membrane as development proceeds. We found that BBs always contacted membranes at the level of Par3-enriched apical junctions. Par3 became enriched at the posterior apical side of FP cells before BB polarization. Par3 overexpression disrupted FP polarization and its localization was disrupted in a *Vangl2* mutant. Thus, we propose that a major role of the PCP pathway in the FP is to drive Par3 asymmetric localization, which in turn mediates BB posterior positioning.

RESULTS

Floor-plate polarization shows temporal progression but no spatial synchronization

Posterior positioning of the BB in the zebrafish FP is visible as soon as 18 hours post-fertilization (hpf) (Mahuzier et al., 2012) and is maintained at least until 72 hpf (Mathewson et al., 2019). From 24 hpf onward, coupled to posterior tilting of cilia, it is instrumental in propelling the CSF in the spinal cord central canal (Borovina et al., 2010, Fame et al., 2016). At late gastrulation stages (10 hpf), ectodermal cells already display a slight posterior bias of centrioles (Sepich et al., 2011). At early somite (s) stages, centrioles have migrated under the apical membrane in several cell types and short cilia are detected with the Arl13b-GFP transgenic line (Borovina et al., 2010).

To define the time-course of FP cell polarization during somitogenesis, we assessed basal-body (BB) position along the antero-posterior (A/P) axis on fixed embryos from the 6 s to the 26 s stage (Fig. 1a, b). For each cell we defined a BB polarization index (p.i. in Fig. 1b). BBs already exhibited a posterior bias at 6 s, since 50% of FP cells had a BB in contact with the apical posterior membrane, and 20% of BBs were located within the posterior third. The polarization state did not change significantly until 10 s. While we could find some FP cells with an anterior BB between the 6 s and 14 s stages (Fig. 1a, yellow arrow), it was not the case later. From 10 s onward, there was a progressive increase in FP polarization, mostly due to an increase in the percentage of cells with a BB in contact with the posterior membrane, with a concomitant disappearance of anterior BBs and a reduction of median BBs. The polarization state of the FP was considered complete at 18 s, since no significant difference could be detected between the 18 s and 26 s stages. Interestingly, we did not detect a gradient of polarization index along the A/P axis of the spinal cord (Fig. S1a), and single non-polarized cells were often intermingled among polarized neighbors (Fig. S1b), arguing against the existence of waves of polarization originating from axis extremities.

BBs are highly mobile in FP cells

We then turned to live-imaging to obtain a dynamic view of the polarization process and assess BB motility within the apical surface and potential correlations with cell deformation and cell division. We used time-lapse movies to follow BB movements within the apical surface of individual FP cells at different developmental stages, ranging from 4 s to 21 s. We found that BBs displayed a highly motile behavior, while remaining located in the most apical cortex (Fig. 1c-f) (Supplementary movies S1-S4). They moved both anteriorly and posteriorly (Fig. S1e, first column), and thus not only toward posterior membranes as could be suggested by the analysis on fixed samples.

BB movements seemed independent of cell deformation. Cell deformations along the AP axis were more important at early stages (4-10 s) (Fig. 1c, d), probably as a consequence of convergence-extension movements (compare for example purple lines of graphs in Fig1d and e), but most BB movements were not correlated with cell deformation (see Fig. 1c). At later stages (14-21 s) (Fig. 1e, f), cell deformations were small and did not correlate with BB movements. One possible explanation for the presence of unpolarized cells next to polarized neighbors is that they could either be in mitosis or soon after mitosis, before BB re-localization. To test this hypothesis, we quantified mitoses and followed daughter cells after cell division. Mitoses were rare in FP cells at early stages (6 mitoses / 79 cells for 9 embryos analyzed at 4-8 s) and absent at later stages (118 cells from 15 embryos at 13-21s). In addition, after cytokinesis, the centriole of the posterior daughter cell returned to the posterior membrane in a very short time (14 min in average, n=6), and so did the centriole of the anterior daughter cell that polarized during the movie (22 min in average, n=3) (Fig. S1d) (Supplementary movie S5). Most of the observed unpolarized cells were in interphase. Thus, we concluded that the state of FP cell polarization was neither correlated to the cell shape changes nor to the cell cycle.

FP polarization involves a change in BB behavior

In order to characterize BB behavioral changes during development, we determined the percentage of time that BBs spent in contact with the posterior membrane (Fig.

1g). At early stages, BBs spent in average 44% of their time in contact with the posterior membrane, whereas at later stages (13-21 s) it reached 70%. This was largely due to an increase in the number of cells in which the BB stayed in contact with the posterior membrane during the whole movie (for example in Fig. 1e). This situation will be referred to as “posteriorly docked BB”, although it is not known whether a physical link between BB and the posterior membrane exists. At early stages (4-8s), we did not observe any cell with posteriorly docked BBs (41 cells analyzed, 5 embryos), whereas they made up around a third (34%) of the FP cell population at 13-17s stages (13/38 cells, 6 embryos) and almost half (46%) the FP population at later stages (17-21s, 27/59 cells, 7 embryos). BB behavioral changes during somitogenesis were also characterized by a decrease in the frequency of BB direction changes, as well as an increase in the mean duration of BB/posterior membrane contact events and mean polarization index, suggesting that, as development proceeds, BB movements are less dynamic and more confined to the posterior side of the cell (Fig. S1e, plots of the first line). Posteriorly docked BBs made a significant contribution to these behavioral changes. In order to determine if changes in the behavior of non-posteriorly docked BB contributed to the increase of FP polarization during somitogenesis, we quantified the same parameters, but taking into account only these motile BBs (Fig. S1e, second line): although less drastic, the same trend in BB behavior change was observed.

To further characterize the behavior of non-posteriorly docked BB, we quantified the frequency of contact events between the BB and either the anterior or the posterior membrane (Fig. 1h and i, respectively). First, posterior contacts were more frequent than anterior ones even at 4-8s (compare Fig. 1h and i), confirming that FP cells already have a posterior polarization bias at these early stages. Second, contacts with the anterior membrane were frequently observed at early stages (50% of BBs make at least one anterior contact per hour, see for example at t=70’ in Fig1d), but almost never observed at later stages (only 3/57 cells display one anterior contact). Contact frequency with the posterior membrane was also significantly higher at earlier stages (1.3 contact/h on average) than at later stages (around 0.8 contacts/hour in average within the 13-21s stage window, Fig. 1i). This reduction in the number of contact events could be due to an increase in their duration (Fig. S1e,

plot 2nd column, 2nd line) and to a reduction in BB speed. Indeed, we found that BBs moved faster at earlier stages (FigS1c, median movement speed was around 0.2μm/min at 4-8 s versus 0.1μm/min at 13-21 s). Thus, the observed changes in FP polarization are explained both by an increase in the posteriorly docked BB population and by behavioral changes (reduced speed, less direction changes, longer posterior contact events) in other BBs.

Interestingly, live-imaging revealed the presence of membrane invaginations extending between the BB and transverse membranes (Supplementary movies S6 and S7). At early stages, we could detect such invaginations in 44% of FP cells (taking into account only non-posteriorly docked BBs) (26 cells out of 59 cells from 9 embryos), most of which were linking the posterior membrane and the BB (78%, 25/32 invagination events, Fig. S2a white arrows) (Movie S6), although invaginations from the anterior membrane were also seen (Fig. S2b, white arrow) (Movie S7). These early stage invaginations were most of the time observed on a single time frame (anterior invaginations) or two consecutive timeframes in time-lapse movies with a 5 min time interval between two images (FigS2c). Posterior invaginations were followed by a posterior directed BB movement in 66% of cases (33/50 invaginations), suggesting a causal link between their formation and movement of the BB to the posterior membrane. BB behavior following anterior invaginations did not seem different from BB behavior after posterior invaginations, but these results need to be confirmed as the number of anterior invaginations was very low (we observed only 14 such events, compared to the 50 posterior invagination events) (FigS2d). Membrane invaginations were rarely seen at later stages (after 14s, 9/40 cells, 10 embryos), probably in part because BBs spent a higher fraction of their time associated with the posterior membrane (see Fig. 1 and Fig. S1).

Overall, our dynamic analysis reveals a highly motile behavior of BBs in FP cells at early somite stages. This was unexpected, given that BBs are already anchored to the apical membrane at early somite stages and have grown a cilium that protrudes externally (Fig. 1a) (Borovina et al., 2010). As somitogenesis proceeds, BBs show decreased mobility. They progressively stop shuttling from anterior to posterior cell junctions and their contacts with the posterior membrane last longer. Importantly,

almost half of them still detach from the posterior membrane but only for short periods of time and remain close to the posterior apical junction.

We therefore made the hypothesis that from the 10s stage, the posterior apical junctions become progressively enriched in proteins that can mediate BB posterior localization.

Posterior enrichment of Par3 precedes BB/posterior membrane contact

In Drosophila, the apical junction protein Par3 modulates centrosome positioning in the male germline and embryonic ectoderm (Inaba et al., 2015, Jiang et al., 2015). In order to test a potential role for Par3 in BB posterior positioning in FP cells, we first assessed Par3 localization by immunostaining (Fig. 2a, b). At the 14 s stage, Par3 localized at apical junctions of FP cells (Fig. 2a). Strikingly, Par3 patches were also detected on transverse membranes (anterior and posterior membranes cannot be distinguished in this experiment) and in close contact with posteriorly docked BBs (white arrows, Fig. 2a). This distribution was confirmed using the BazP1085 antibody (Fig. 2b), which recognizes a conserved Par3 phosphorylation site targeted by Par1 (Krahn et al. 2009). Interestingly, Par3 transversal patches were also present in FP cells in which the BB was not yet in contact with the posterior membrane (Fig. 2a, b, right panels) showing that this enrichment precedes stable BB/posterior membrane contact establishment.

In order to test whether Par3 is asymmetrically enriched in FP cells, we used a mosaic expression approach of Par3-RFP and centrin-GFP fusions in live embryos. Quantification of Par3 expression showed that, among fully polarized (p.i. =1) individual Par3-RFP expressing FP cells, both at early (6-12s, Fig. 2c, left) and late (14-20s, Fig. 2c, right) stages, almost all cells had a Par3-RFP post/ant ratio greater than 1 (Fig. 2d) (29/30 cells out of 20 embryos; 6-12s, mean ratio= 1.42, N=7, n=9; 14-20s mean ratio =1.38, N=13, n=21). To determine whether the enrichment of Par3 at the posterior membrane preceded BB/posterior membrane contact, we made movies of BB movements and quantified Par3-RFP posterior/anterior ratio at each time-point; we found that Par3-RFP was enriched posteriorly before the BB contacts the posterior membrane (Fig. 2e, f) (12/14 cells from 12 embryos) (Supplementary

movies S8 and S9). In contrast, BBs of FP cells with weak or no posterior Par3 enrichment tended to remain unpolarized (either making no contact (2/5 cells, 5 embryos) or unstable contacts (3/5 cells, 5 embryos) with the posterior membrane (Fig. 2g) (Supplementary movie S10).

Thus, we show that Par3 forms patches at FP apical transverse membranes and that BBs are posteriorly docked at these patches. We further show that Par3 is enriched posteriorly before BB/posterior membrane contact. Together, our data strongly suggest that Par3 is a key player in mediating BB positioning at the posterior membrane, by attracting it and/or holding it when it contacts the posterior membrane.

At early stages, BBs contact transverse membranes exclusively at Par3 patches

During the second half of somitogenesis, Par3 tended to form a continuous belt at apical junctions of FP cells, although it was locally enriched, forming patches that associated with centrosomes as described above. In contrast, at the 4 to 8 s stages, Par3 formed small, discrete patches at FP apical transverse membranes, but not at lateral membranes. These patches were roughly aligned with the AP axis of the embryo (Fig. 3a, white arrows). Strikingly, BBs made contacts with anterior and posterior transverse membranes (as described in Fig. 1) exclusively at the level of these patches (58 cells from 18 embryos) as shown in Fig. 3b and Supplementary movie S11. In 33% of these cells (19/58), the discrete Par3 patches stretched toward the BB (for example, Fig. 3b yellow arrows). In about 25% of these stretched patches (5/19) we could detect an underlying membrane digitation originating from either the posterior (Fig. 3c, t=0') or the anterior membrane (Fig. 3c, t=64') and extending toward the BB (Supplementary movie S12). The presence of membrane digitations and their overlap with Par3 patches point to the existence of mechanical forces between BBs and membranes at the level of Par3 patches and suggests that Par3 could be required for local force generation.

Par3 over-expression disrupts BB positioning

To test whether Par3 is required for posterior BB positioning in the FP, we first used a loss-of-function approach. MO-mediated knock-down of Par3ab (also known as Pard3 or ASIP) did not disrupt FP PCP (Fig. S3a), nor could we see a defect in a *MZpar3ab* mutant (Blasky et al., 2014) (Fig. S3c). However, in both cases, Par3 patches could still be detected in the FP by immunostaining (Fig. S3b, d- g), suggesting that *par3ab* loss-of-function was compensated for by its paralogous genes (*par3aa*, *par3ba* or *par3bb*), which could also be detected by our Par3 antibodies thanks to the high conservation of the epitopes. We thus turned to an over-expression approach to disrupt Par3 posterior enrichment and patch formation. Over-expressed Par3-RFP in the floor-plate localized to apical junctions and did not disrupt apico-basal polarity, as assessed by the presence of the BB at the apical surface and the proper localization of the apical junction protein ZO1 (Fig. S3e). In contrast to MbCherry over-expression taken as a control, Par3-RFP over-expression disrupted BB posterior positioning in the FP (Fig. 3d, MbCherry median p.i.=1, first quartile=0.94; Par3-RFP median p.i.=0.8, first quartile=0.64). Furthermore, mosaic over-expression showed that this effect was cell autonomous, as there was no significant difference in BB positioning between Par3-RFP negative cells in Par3-RFP expressing embryos and MbCherry negative cells in MbCherry expressing embryos (Fig. 3d MbCherry median p.i.=1, first quartile=0.84; Par3-RFP median p.i.=1, first quartile= 0.83).

These results strongly suggest that Par3 posterior enrichment and patch formation are required for proper BB positioning in the FP.

Par3 clustering and localization is disrupted in the *vangl2* mutant FP

Vangl2, a core PCP protein, has been shown to be involved in PCP in the zebrafish FP (Borovina et al., 2010) but the downstream mechanisms linking Vangl2 to centrosome posterior positioning are unknown. We thus analyzed the dynamics of FP polarization in the *vangl2*^{m209} (initially called *trf*^{m209}) mutant (Solnica-Krezel et al., 1996). At 18 s, the BB of *vangl2*$^{m209/m209}$ FP cells was mispositioned at the center of the apical cell surface, while *vangl2*$^{m209/+}$ embryos had normally polarized BBs as judged by immunostaining (median p.i.=0.6 versus 1 for wt or *vangl2*$^{m209/+}$) (Fig. 4a,

FP polarization plot). Live-imaging of *vangl2*$^{m209/m209}$ FP revealed that BBs maintained a high motility at late stages. In addition, most *vangl2*$^{m209/m209}$ BBs made at least one contact with either transverse or lateral membranes (70%, 17/25), suggesting that force generators are still present in these mutants but more dispersed around the cell periphery.

To test whether Vangl2 could impact Par3 function in this process, we looked at phospho-Par3 localization in the *vangl2* mutant. Phospho-Par3 localized at apical junctions in *vangl2*$^{m209/m209}$ as in controls (Fig. 4b). Automatic detection of Par3 patches along the transverse apical junctions revealed that in wt, 90% of FP cells had at least a major phospho-Par3 patch (Fig. 4b, yellow arrows), with 39% of cells also having smaller secondary patches (Fig. 4c, N=7, n=186). In *vangl2*$^{m209/m209}$ embryos, the number of FP cells with at least one phospho-Par3 patch was unchanged (around 90% of cells) but the number of cells with more than one patch was increased (54% of cells, N=7, n=129). In addition, the prominence of phospho-Par3 patches fluorescence intensity was decreased in *vangl2*$^{m209/m209}$ embryos as compared to controls (see Fig. 4d for prominence definition and quantification). Similar results were obtained with the antibody against total Par3, although the changes in prominence were not statistically significant in this case. Thus, Par3 forms more numerous and smaller patches in *Vangl2* mutants, showing a role for Vangl2 in Par3 clustering.

To analyze BB behavior in *vangl2* mutants and test whether Par3 localization was affected in *vangl2*$^{m209/m209}$ FP cells, we made time-lapse movies of embryos mosaically injected with Par3-RFP (Fig. 4e, f) (Supplementary movies S13 and S14). In *vangl2* mutants, FP cells displayed motile BBs that contacted the membrane at the level of Par3 patches, but the distribution of the patches was very different. Compared to control embryos (*vangl2*$^{+/+}$ and *vangl2*$^{m209/+}$), *vangl2*$^{m209/m209}$ embryos at 4-8s displayed more cells with an anterior Par3 patch (82% vs 67%) and less cells with a posterior patch (65% vs 87%). In addition, lateral Par3 patches were much more common in *vangl2* mutants (70% vs 20%, *vangl2*$^{m209/m209}$: N=7, n=17; controls : N=16, n=45, Fig. 4g). These results show that Vangl2 is required for proper positioning of Par3 patches at early stages. Interestingly, live-imaging of these embryos also revealed that, despite Par3 mislocalization, BB still made contact with

membranes exclusively at Par3 patches (Fig. 4e, f) independently of their position, whether laterally (Fig. 4e) or posteriorly (Fig. 4f). These observations show that Par3 distribution along apical junctions is disrupted in *vangl2* mutants, leading to a fragmentation of Par3 patches into more numerous and less intense clusters that extend to lateral membrane.

DISCUSSION

In this paper we have analyzed the dynamics of BB posterior positioning in the embryonic zebrafish FP. We show that, quite unexpectedly, BBs are highly mobile and are able to contact, and bounce off, apical junctions several times per hour. FP polarization correlates with slowing down of BBs. At the level of individual cells, BBs settle down posteriorly at the level of junctions enriched in Par3, and we show that Par3 is important for BB posterior localization. In the PCP mutant *Vangl2*, BBs show poorly oriented movements and this correlates with Par3 mislocalization. We discuss here the implications of our dynamic study on the understanding of the mechanisms of cilium polarization downstream of the PCP pathway. Our data highlight Par3 as a critical player in centriole positioning in this system.

Analysis of fixed samples showed that posterior positioning of BBs within the apical surface of FP cells progressed regularly within the 8 hour-time frame of our study and was complete at the 18 s stage. Surprisingly, live imaging revealed that, during this time frame, BBs underwent active antero-posterior movements under the apical surface, in both directions. This contrasts with the situation in the mouse cochlea, where live-imaging of explants had suggested very slow and regular movements of the BBs to the lateral cortex of inner hair cells (estimated speed of 10-50 nm/h, undetectable in movies) (Lepelletier et al., 2013). The BB speed measured in our experiments (median speed of 0.2 μm/min at early stages of polarization) is closer to that of the second phase of centrosome migration toward the immune-synapse in T cells, when the centrosome approaches the actin rich cortex that faces the target cell (1 μm/min) (Yi et al., 2013). This suggests that BB movements in FP cells could rely on mechanisms similar to those found in T lymphocytes, where end-on capture-shrinkage of microtubules by dynein at the immune synapse pulls the centrosome. A striking difference between these two processes is the presence of a growing cilium

anchored to the distal part of the BB in FP cells. Thus, it is likely that the presence of a cilium does not have a major impact on BB movement.

The lack of synchronization between adjacent cells and of long-range temporal gradient of BB polarization suggests that the timing of polarization is largely dependent on cell-intrinsic cues. Cell division did not appear to have a major role in the timing of polarization. Thus, we proposed the maturation of cell junctions as a possible trigger of polarization. Accordingly, we found that Par3 accumulated in patches at the posterior apical junctions of FP cells and that this accumulation preceded BB posterior docking. Interestingly, several recent studies suggest that Par3 could have a widely conserved role in PCP: Par3 is asymmetrically localized within the plane of the epithelium in Drosophila ommatidia (Aigouy et al., 2016), in Xenopus embryo ectoderm (Chuykin et al., 2019) and in the mouse cochlea (Landin Malt et al., 2019). Beside their asymmetric enrichment in polarized tissues, Par3 clusters may be broadly involved in BB/centrioles recruitment. Indeed, In the mouse cochlea, Par3 transiently localizes to the abneural membrane of hair cells and is required for proper BB localization (Landin Malt et al., 2019). Moreover, in Drosophila early gastrula ectoderm, Par3 isotropic distribution around apical junctions contributes to epithelium integrity, but in aPKC loss of function mutants, Par3 accumulates as discrete patches that align along the dorso-ventral axis and recruit centrosomes (Jiang et al., 2015). Centrosome docking at discrete Par3 patches has also been observed in Drosophila germ stem cells and is critical for proper division orientation (Inaba et al., 2015).

Our analysis of the *vangl2* mutant defective in FP polarity brings important insight into the role of Par3 in FP polarization. In *vangl2*$^{m209/m209}$ embryos, BBs showed less oriented movements than in wt embryos. In contrast to the wt situation, BBs contacted both transverse and lateral membranes. Strikingly, in *vangl2* mutants as in wt, BBs always contacted the apical junctions at the level of Par3-positive patches. The altered behavior of BBs in *vangl2*$^{m209/m209}$ embryos correlated with a mislocalization of Par3 around the apical junctions of FP cells. Since Par3 overexpression affected BB polarization, we propose that Par3 posterior enrichment under the control of the PCP pathway is a main actor in BB posterior positioning.

How PCP proteins act on Par3 localization in the FP remains to be uncovered. In FP cells, Vangl2 localizes anteriorly (Davey et al. 2016), suggesting that its effect on Par3 localization is indirect. Vangl2 effect on Par3 could be mediated by Dvl, since it is required for proper asymmetric localization of Dvl in planar polarized tissues and Dvl, together with Meru, can recruit Par3 to sensory organ precursor posterior membrane in Drosophila (Banerjee et al. 2017). Dvl could also recruit Par3 via Daple, as this protein colocalizes with Par3 in the mouse cochlea and can bind both Dvl and Par3 in yeast two-hybrid assays (Siletti et al. 2017).

The mechanisms by which Par3 can recruit the BB at the plasma membrane are unknown. Par3 enrichment could attract the BB to the posterior membrane or, alternatively, could capture or hold it when it contacts the posterior membrane. The observation of membrane invaginations suggests the existence of mechanical forces between Par3-positive patches and BBs. Such membrane invaginations have been previously observed during cell division in the *C. elegans* zygote (Redemann et al., 2010) and in the *C. intestinalis* embryo epidermal lineage (Negishi et al., 2016), as well as at the immunological synapse in T cells (Yi et al., 2013). In all three cases, the existence of attraction forces between the centriole and the membrane has been proposed.

Microtubules were recently shown to be instrumental in FP polarity maintenance at late stages (30 to 72 hours post fertilization, Mathewson et al. 2019) and our results suggest that they could also be involved in polarity establishment. Indeed, BB movement toward the posterior Par3 patches could involve local microtubule dynamics regulation, since Par3 can interact with Dynein (Schmoranzer et al., 2009) and also with microtubules, directly (Chen et al., 2013) or indirectly via 14-3-3 proteins (Benton et al., 2003). Interestingly, we found that a form of Par3 phosphorylated at two conserved serine residues is enriched at posterior junctions. This phosphorylation site is a target of the Par1 kinase. It plays a role in centrosome recruitment at Par3 patches in Drosophila (Jiang et al., 2015) and in the interaction of Par3 with 14-3-3 proteins and thus with microtubules in other systems (Benton et al., 2003).

Par3 could also act indirectly on microbutules via Rac1, which mediates Par3 function in the mouse cochlea (Landin Malt et al., 2019). In different systems, Par3 regulates the local activity of Rac via the RacGEFs Tiam1 and Trio (Nishimura et al., 2005, Matsuzawa et al., 2016). Par3 can increase microtubule catastrophe rate by inhibiting Trio in neural crest cells (Moore et al., 2013), and Rac1 can regulate microtubule dynamics via CLIP-170 or Stathmin in other systems (Fukata et al., 2002, Wittmann et al., 2004).

Asymmetric centriole positioning is now recognized as a conserved readout of PCP (Carvajal-Gonzalez 2016). It will be interesting to investigate whether Par3 has a conserved role in centriole/BB positioning in metazoans.

MATERIALS AND METHODS

Experimental model and subject details

Wild-type and mutant zebrafish embryos were obtained by natural spawning. To obtain the early stages (4-8s), embryos were collected at 10 am and incubated for 9 h in a 33°C incubator. To obtain later stages (14-20s), embryos were collected at 10 am and incubated for 2 h at 28 °C before being placed overnight in a 24 °C incubator. All our experiments were made in agreement with the european Directive 210/63/EU on the protection of animals used for scientific purposes, and the french application decree 'Décret 2013-118'. The projects of our group have been approved by our local ethical committee 'Comité d'éthique Charles Darwin'. The authorisation number is 2015051912122771 v7 (APAFIS#957). The fish facility has been approved by the French 'Service for animal protection and health' with approval number A-75-05-25.

Method details

mRNA and morpholino injection

mRNAs were synthesized from linearized pCS2 vectors using the mMESSAGE mMACHINE SP6 transcription kit (Ambion). The following amounts of mRNA were injected into one-cell stage embryos: 22pg for Centrin-GFP, 40 pg for mbCherry (membrane Cherry) or Membrane-GFP (Gap43-GFP). For Par3-RFP mosaic expression, mRNAs were injected at the 16 cell stage in a single blastomere, using 50pg for Par3-RFP live-imaging or 150pg Par3-RFP for over-expression experiments (the concentrations for Centrin-GFP and membrane-GFP mRNAs were the same as for one-cell stage injections). Par3-MO was injected at a concentration of 0.3mM at one-cell stage.

Immunostaining

For immunostaining, embryos were fixed in Dent fixative (80% Methanol, 20% DMSO) at 25°C for 2h, blocked in 5% goat serum, 1% bovine serum albumin and 0.3% triton in PBS for 1 h at room temperature and incubated overnight at 4 °C with primary antibodies and 2h at room temperature with secondary antibodies. The yolk

was then removed and the embryo mounted in Vectashield medium on a slide. Imaging was done using a Leica TCS SP5 AOBS upright confocal microscope using a 63X oil lens.

Live imaging.

Embryos were dechorionated manually and mounted in 0.5% low-melting agarose in E3 medium. Movies were recorded at the temperature of the imaging facility room (22 °C) on a Leica TCS SP5 AOBS upright confocal microscope using a 63X (NA 0.9) water immersion lens.

Quantification and statistical analysis

All bar-plots, boxplot and violin plots and statistical tests were generated with R and Rstudio.

Basal-bodies movements

Distance between BB and posterior membrane in FP was measured manually at each time-frame in FIJI. The results were then plotted using python matplotlib and analyzed with a custom python script to extract relevant information such as the frequency of contact with posterior membrane or percentage of total time spent in contact with posterior membrane.

Par3-RFP posterior/anterior ratio

Fluorescence intensity was measured along the anterior-posterior length of isolated labelled FP cells in FIJI. A custom python script was then used to extract the first quarter (cell anterior side) and last quarter (cell posterior side) of fluorescence intensity values, to determine the area under each curve (corresponding to fluorescence intensity), calculate the post/ant ratio and plot it along with the polarization index (see BB movements analysis section).

Par3 peaks quantification

Fluorescence intensity from immunostained embryos was measured along FP cells transverse membranes and exported to Matlab where the findpeaks function was used to detect Par3 peaks and measure their prominence.

REAGENTS AND RESOURCES

Reagent type or resource	Designation	Source or reference	Identifiers	Additional information
Antibody	Mouse monoclonal IgG2a anti-centrin (clone 20H5)	Merck Millipore	# 04-1624 RRID: AB_10563501	1:200 dilution
Antibody	Mouse monoclonal IgG1 anti-ZO1 (clone ZO1-1A12)	Invitrogen	RRID: AB_2533147	1:400 dilution
Antibody	Mouse monoclonal IgG2b anti-acetylated-tubulin (clone 6-11B-1)	Sigma-Aldrich	#T 6793 RRID: AB_477585	1:400 dilution
Antibody	Rabbit polyclonal anti-Par3	Merck Millipore	#07-330 RRID:AB_11213581	1:200 dilution
Antibody	Rabbit polyclonal anti-phosphorylated-Ser1085-Bazooka	Krahn et al. 2009	N/A	1:200 dilution
Antibody	Rabbit polyclonal anti-DsRed	Takara	# 632496 RRID:AB_10013483	1:400 dilution
Antibody	Goat anti-mouse IgG1 Alexa633	Molecular probes	# A-21126 RRID:AB_2535768	1:400 dilution
Antibody	Goat anti-mouse IgG2a Alexa568	Molecular probes	# A-21134 RRID:AB_2535773	1:400 dilution
Antibody	Goat anti-mouse IgG2a Alexa488	Molecular probes	# A-21131 RRID:AB_141618	1:400 dilution
Antibody	Goat anti-mouse IgG2b Alexa633	Molecular probes	# A-21146 RRID:AB_2535782	1:400 dilution
Antibody	Goat anti-rabbit IgG Alexa568	Molecular probes	# A-11011 RRID:AB_143157	1:400 dilution
Chemical	Methanol	VWR Chemicals	20847.295	
Chemical	DMSO	Sigma	D2650	
Chemical	Goat serum	Sigma	G6767	

Chemical	Bovine serum albumin	Sigma	A2153	
Chemical	Triton X100	Sigma	T8787	
Chemical	Vectashield	Vector Laboratories	H-1000	
Strain (Danio rerio)	zebrafish wild-type AB or (TL x AB) hybrid strains	N/A	N/A	
Strain (Danio rerio)	Zebrafish Vangm209 mutants	Solnica-Krezel et al., 1996	ZDB-GENO-190204-5	
Strain (Danio rerio)	Zebrafish Par3ab fh305 mutants	Blasky et al., 2014	ZDB-FISH-150901-20689	
Oligonucleotide	Par3-MO tcaaaggctcccgtgctctggtgtc	Wei et al., 2004		
Recombinant DNA	pCS2-Membrane-Cherry	Megason et al. 2009	N/A	
Recombinant DNA	pCS2-GFPhumcentrin1	Pouthas et al. 2008	N/A	
Recombinant DNA	pCS2+-Par3-RFP	Paula Alexandre, unpublished	N/A	
Recombinant DNA	pCS-Gap43-GFP	David Wilkinson, unpublished	N/A	
Software	Fiji/ImageJ	ImageJ	https://imagej.net/Fiji/Downloads	
Software	MATLAB R2018a	Mathworks	https://www.mathworks.com/downloads/	
Software	Python 2.7.13	Python Software Foundation	https://www.python.org/downloads/release/python-2713/	
Software	R studio Version 1.1.463	Rstudio	https://www.rstudio.com/	
Software	R version 3.3.2	The R Foundation for Statistical Computing	https://cran.r-project.org/bin/macosx/	

1

2

3

BIBLIOGRAPHY

Aigouy B, Le Bivic A. The PCP pathway regulates Baz planar distribution in epithelial cells. Sci Rep. 2016 Sep 14;6:33420. doi: 10.1038/srep33420.

Banerjee JJ, Aerne BL, Holder MV, Hauri S, Gstaiger M, Tapon N. Meru couples planar cell polarity with apical-basal polarity during asymmetric cell division. *eLife Sciences* **6**, e25014 (2017). doi: 10.7554/eLife.25014

Benton R, St Johnston D. Drosophila PAR-1 and 14-3-3 inhibit Bazooka/PAR-3 to establish complementary cortical domains in polarized cells. Cell. 2003 Dec 12;115(6):691-704.

Blasky AJ, Pan L, Moens CB, Appel B. Pard3 regulates contact between neural crest cells and the timing of Schwann cell differentiation but is not essential for neural crest migration or myelination. Dev Dyn. 2014 Dec;243(12):1511-23. doi: 10.1002/dvdy.24172.

Borovina A, Superina S, Voskas D, Ciruna B. Vangl2 directs the posterior tilting and asymmetric localization of motile primary cilia. Nat Cell Biol. 2010 Apr;12(4):407-12. doi: 10.1038/ncb2042.

Boutin C, Goffinet AM, Tissir F. Celsr1-3 cadherins in PCP and brain development. Curr Top Dev Biol. 2012;101:161-83. doi: 10.1016/B978-0-12-394592-1.00010-7.

Carvajal-Gonzalez JM, Mulero-Navarro S, Mlodzik M. Centriole positioning in epithelial cells and its intimate relationship with planar cell polarity. Bioessays. 2016 Dec;38(12):1234-1245. doi: 10.1002/bies.201600154.

Chen S, Chen J, Shi H, Wei M, Castaneda-Castellanos DR, Bultje RS, Pei X, Kriegstein AR, Zhang M, Shi SH. Regulation of microtubule stability and organization by mammalian Par3 in specifying neuronal polarity. Dev Cell. 2013 Jan 14;24(1):26-40. doi: 10.1016/j.devcel.2012.11.014.

Chuykin I, Ossipova O, Sokol SY. Par3 interacts with Prickle3 to generate apical PCP complexes in the vertebrate neural plate. Elife. 2018 Sep 26;7. pii: e37881. doi: 10.7554/eLife.37881.

Davey, C. F., Mathewson, A. W. & Moens, C. B. PCP Signaling between Migrating Neurons and their Planar-Polarized Neuroepithelial Environment Controls Filopodial Dynamics and Directional Migration. PLOS Genetics 12, e1005934 (2016).

Ezan J, Lasvaux L, Gezer A, Novakovic A, May-Simera H, Belotti E, Lhoumeau AC, Birnbaumer L, Beer-Hammer S, Borg JP, Le Bivic A, Nürnberg B, Sans N, Montcouquiol M. Primary cilium migration depends on G-protein signalling control of subapical cytoskeleton. Nat Cell Biol. 2013 Sep;15(9):1107-15. doi: 10.1038/ncb2819.

Fame RM, Chang JT, Hong A, Aponte-Santiago NA, Sive H. Directional cerebrospinal fluid movement between brain ventricles in larval zebrafish. Fluids Barriers CNS. 2016 Jun 21;13(1):11. doi: 10.1186/s12987-016-0036-z.

Fukata M, Watanabe T, Noritake J, Nakagawa M, Yamaga M, Kuroda S, Matsuura Y, Iwamatsu A, Perez F, Kaibuchi K. Rac1 and Cdc42 capture microtubules through IQGAP1 and CLIP-170. Cell. 2002 Jun 28;109(7):873-85.

Grimsley-Myers CM, Sipe CW, Géléoc GS, Lu X. The small GTPase Rac1 regulates auditory hair cell morphogenesis. J Neurosci. 2009 Dec 16;29(50):15859-69. doi: 10.1523/JNEUROSCI.3998-09.2009.

Guirao B, Meunier A, Mortaud S, Aguilar A, Corsi JM, Strehl L, Hirota Y, Desoeuvre A, Boutin C, Han YG, Mirzadeh Z, Cremer H, Montcouquiol M, Sawamoto K, Spassky N. Coupling between hydrodynamic forces and planar cell polarity orients mammalian motile cilia. Nat Cell Biol. 2010 Apr;12(4):341-50. doi: 10.1038/ncb2040.

Hashimoto M, Shinohara K, Wang J, Ikeuchi S, Yoshiba S, Meno C, Nonaka S, Takada S, Hatta K, Wynshaw-Boris A, Hamada H. Planar polarization of node cells determines the rotational axis of node cilia. Nat Cell Biol. 2010 Feb;12(2):170-6. doi: 10.1038/ncb2020.

Hegan PS, Ostertag E, Geurts AM, Mooseker MS. Myosin Id is required for planar cell polarity in ciliated tracheal and ependymal epithelial cells. Cytoskeleton (Hoboken). 2015 Oct;72(10):503-16. doi: 10.1002/cm.21259.

Hirota Y, Meunier A, Huang S, Shimozawa T, Yamada O, Kida YS, Inoue M, Ito T, Kato H, Sakaguchi M, Sunabori T, Nakaya MA, Nonaka S, Ogura T, Higuchi H, Okano H, Spassky N, Sawamoto K. Planar polarity of multiciliated ependymal cells involves the anterior migration of basal bodies regulated by non-muscle myosin II. Development. 2010 Sep;137(18):3037-46. doi: 10.1242/dev.050120.

Inaba M, Venkei ZG, Yamashita YM. The polarity protein Baz forms a platform for the centrosome orientation during asymmetric stem cell division in the Drosophila male germline. Elife. 2015 Mar 20;4. doi: 10.7554/eLife.04960.

Jiang T, McKinley RF, McGill MA, Angers S, Harris TJ. A Par-1-Par-3-Centrosome Cell Polarity Pathway and Its Tuning for Isotropic Cell Adhesion. Curr Biol. 2015 Oct 19;25(20):2701-8. doi: 10.1016/j.cub.2015.08.063. Epub 2015 Oct 8.

Jones C, Roper VC, Foucher I, Qian D, Banizs B, Petit C, Yoder BK, Chen P. Ciliary proteins link basal body polarization to planar cell polarity regulation. Nat Genet. 2008 Jan;40(1):69-77.

Landin Malt A, Dailey Z, Holbrook-Rasmussen J, Zheng Y, Hogan A, Du Q, Lu X. Par3 is essential for the establishment of planar cell polarity of inner ear hair cells.

Proc Natl Acad Sci U S A. 2019 Mar 12;116(11):4999-5008. doi: 10.1073/pnas.1816333116.

Lepelletier L, de Monvel JB, Buisson J, Desdouets C, Petit C. Auditory hair cell centrioles undergo confined Brownian motion throughout the developmental migration of the kinocilium. Biophys J. 2013 Jul 2;105(1):48-58. doi: 10.1016/j.bpj.2013.05.009.

Mahuzier A1, Gaudé HM, Grampa V, Anselme I, Silbermann F, Leroux-Berger M, Delacour D, Ezan J, Montcouquiol M, Saunier S, Schneider-Maunoury S, Vesque C. Dishevelled stabilization by the ciliopathy protein Rpgrip1l is essential for planar cell polarity. J Cell Biol. 2012 Sep 3;198(5):927-40. doi: 10.1083/jcb.201111009.

Mathewson AW, Berman DG, Moens CB. Microtubules are required for the maintenance of planar cell polarity in monociliated floorplate cells. Dev Biol. 2019 Apr 25. pii: S0012-1606(18)30742-5. doi: 10.1016/j.ydbio.2019.04.007.

Matsuzawa K, Akita H, Watanabe T, Kakeno M, Matsui T, Wang S, Kaibuchi K. PAR3-aPKC regulates Tiam1 by modulating suppressive internal interactions. Mol Biol Cell. 2016 May 1;27(9):1511-23. doi: 10.1091/mbc.E15-09-0670.

Megason SG. In toto imaging of embryogenesis with confocal time-lapse microscopy. Methods Mol Biol. 2009;546:317-32. doi: 10.1007/978-1-60327-977-2_19.

Meunier A, Azimzadeh J. Multiciliated Cells in Animals. Cold Spring Harb Perspect Biol. 2016 Dec 1;8(12). pii: a028233. doi: 10.1101/cshperspect.a028233.

Mirzadeh Z, Han YG, Soriano-Navarro M, García-Verdugo JM, Alvarez-Buylla A. Cilia organize ependymal planar polarity. J Neurosci. 2010 Feb 17;30(7):2600-10. doi: 10.1523/JNEUROSCI.3744-09.2010.

Mitchell B, Stubbs JL, Huisman F, Taborek P, Yu C, Kintner C. The PCP pathway instructs the planar orientation of ciliated cells in the Xenopus larval skin. Curr Biol. 2009 Jun 9;19(11):924-9. doi: 10.1016/j.cub.2009.04.018.

Montcouquiol M, Rachel RA, Lanford PJ, Copeland NG, Jenkins NA, Kelley MW. Identification of Vangl2 and Scrb1 as planar polarity genes in mammals. Nature. 2003 May 8;423(6936):173-7.

Moore R, Theveneau E, Pozzi S, Alexandre P, Richardson J, Merks A, Parsons M, Kashef J, Linker C, Mayor R. Par3 controls neural crest migration by promoting microtubule catastrophe during contact inhibition of locomotion. Development. 2013 Dec;140(23):4763-75. doi: 10.1242/dev.098509.

Negishi T, Miyazaki N, Murata K, Yasuo H, Ueno N. Physical association between a novel plasma-membrane structure and centrosome orients cell division. Elife. 2016 Aug 9;5. pii: e16550. doi: 10.7554/eLife.16550.

Nishimura T, Yamaguchi T, Kato K, Yoshizawa M, Nabeshima Y, Ohno S, Hoshino M, Kaibuchi K. AR-6-PAR-3 mediates Cdc42-induced Rac activation through the Rac GEFs STEF/Tiam1. Nat Cell Biol. 2005 Mar;7(3):270-7.

Ohata S, Herranz-Pérez V, Nakatani J, Boletta A, García-Verdugo JM, Álvarez-Buylla A. Mechanosensory Genes Pkd1 and Pkd2 Contribute to the Planar Polarization of Brain Ventricular Epithelium. J Neurosci. 2015 Aug 5;35(31):11153-68. doi: 10.1523/JNEUROSCI.0686-15.2015.

Pouthas F, Girard P, Lecaudey V, Ly TB, Gilmour D, Boulin C, Pepperkok R, Reynaud EG. In migrating cells, the Golgi complex and the position of the centrosome depend on geometrical constraints of the substratum. J Cell Sci. 2008 Jul 15;121(Pt 14):2406-14. doi: 10.1242/jcs.026849.

Redemann S, Pecreaux J, Goehring NW, Khairy K, Stelzer EH, Hyman AA, Howard J. Membrane invaginations reveal cortical sites that pull on mitotic spindles in one-cell C. elegans embryos. PLoS One. 2010 Aug 20;5(8):e12301. doi: 10.1371/journal.pone.0012301.

Ross AJ, May-Simera H, Eichers ER, Kai M, Hill J, Jagger DJ, Leitch CC, Chapple JP, Munro PM, Fisher S, Tan PL, Phillips HM, Leroux MR, Henderson DJ, Murdoch JN, Copp AJ, Eliot MM, Lupski JR, Kemp DT, Dollfus H, Tada M, Katsanis N, Forge A, Beales PL. Disruption of Bardet-Biedl syndrome ciliary proteins perturbs planar cell polarity in vertebrates. Nat Genet. 2005 Oct;37(10):1135-40.

Schmoranzer J, Fawcett JP, Segura M, Tan S, Vallee RB, Pawson T, Gundersen GG.
Par3 and dynein associate to regulate local microtubule dynamics and centrosome orientation during migration. Curr Biol. 2009 Jul 14;19(13):1065-74. doi: 10.1016/j.cub.2009.05.065.

Sepich DS, Usmani M, Pawlicki S, Solnica-Krezel L. Wnt/PCP signaling controls intracellular position of MTOCs during gastrulation convergence and extension movements. Development. 2011 Feb;138(3):543-52. doi: 10.1242/dev.053959.

Siletti, K., Tarchini, B. & Hudspeth, A. J. Daple coordinates organ-wide and cell-intrinsic polarity to pattern inner-ear hair bundles. *Proceedings of the National Academy of Sciences* 201716522 (2017). doi:10.1073/pnas.1716522115

Solnica-Krezel L1, Stemple DL, Mountcastle-Shah E, Rangini Z, Neuhauss SC, Malicki J, Schier AF, Stainier DY, Zwartkruis F, Abdelilah S, Driever W. Mutations affecting cell fates and cellular rearrangements during gastrulation in zebrafish. Development. 1996 Dec;123:67-80.

Song H, Hu J, Chen W, Elliott G, Andre P, Gao B, Yang Y. Planar cell polarity breaks bilateral symmetry by controlling ciliary positioning. Nature. 2010 Jul 15;466(7304):378-82. doi: 10.1038/nature09129.

Tarchini B, Jolicoeur C, Cayouette M. A molecular blueprint at the apical surface establishes planar asymmetry in cochlear hair cells. Dev Cell. 2013 Oct 14;27(1):88-102. doi: 10.1016/j.devcel.2013.09.011.

Wallingford JB. Planar cell polarity signaling, cilia and polarized ciliary beating. Curr Opin Cell Biol. 2010 Oct;22(5):597-604. doi: 10.1016/j.ceb.2010.07.011.

Wei X, Cheng Y, Luo Y, Shi X, Nelson S, Hyde DR. The zebrafish Pard3 ortholog is required for separation of the eye fields and retinal lamination. Dev Biol. 2004 May 1;269(1):286-301.

Wittmann T, Bokoch GM, Waterman-Storer CM. Regulation of microtubule destabilizing activity of Op18/stathmin downstream of Rac1. J Biol Chem. 2004 Feb 13;279(7):6196-203.

Krahn MP, Egger-Adam D, Wodarz A. PP2A antagonizes phosphorylation of Bazooka by PAR-1 to control apical-basal polarity in dividing embryonic neuroblasts. Dev Cell. 2009 Jun;16(6):901-8. doi: 10.1016/j.devcel.2009.04.011.

Yi J, Wu X, Chung AH, Chen JK, Kapoor TM, Hammer JA. Centrosome repositioning in T cells is biphasic and driven by microtubule end-on capture-shrinkage. J Cell Biol. 2013 Sep 2;202(5):779-92. doi: 10.1083/jcb.201301004.

ACKNOWLEDGEMENTS

We are grateful to the aquatic animal and cell imaging facilities of the IBPS (Institut de Biologie Paris-Seine FR3631, Sorbonne Université, CNRS, Paris, France) for their technical assistance. We thank Teresa Ferraro for sharing her expertise in image analysis, Marie Breau for her help in setting up the live imaging protocol, Isabelle Anselme for participation in genotyping. We thank Paula Alexandre for the kind gift of Par3-RFP construct, Andreas Wodarz for the BazP1085 antibody, Maximilien Furthauer for the *vangl2*^{m209} line. We thank Nicolas David and Marie Breau for critical reading and insightful comments on the manuscript. This work was supported by funding from the Agence Nationale pour la Recherche (ANR, project CILIAINTHEBRAIN to SSM) and the Fondation pour la Recherche Médicale (Equipe FRM DEQ20140329544 funding to SSM). A.D was supported by fellowships from the Ecole Normale Supérieure de Cachan and from the Fondation ARC contre le Cancer. The authors declare no competing financial interests.

FIGURE LEGENDS

Figure 1 Floor-plate planar polarization involves a change in basal body (BB) motile behavior.

a, b) Time-course of floor-plate polarization between the 6 s and 26 s stages **a)** Dorsal views of the floor-plate of flat-mounted embryos showing immunostaining against Centrin (green, BB), ZO1 (magenta, apical junctions) and Acetylated-Tubulin (white, cilia) at 12 s (up) and 26 s (down). Note that cilia are already visible at 12 s but are much longer at 26 s. The yellow arrow points at an anterior BB associated to a cilium. **b)** Quantification of BB position measured from immuno-stained samples as shown in a. BB position along the anterior-posterior axis was quantified using the polarization index (defined as p.i.=1-(a/b) where “a” is the distance between the BB and the posterior membrane and “b” the distance between anterior and posterior membranes, cf scheme in b lower right). Cells were then allocated to different categories depending on their polarization index for each developmental stage (6 s: 7embryos, 108 cells ; 8 s: 14 embryos, 224 cells ; 10 s: 14 embryos, 354 cells ; 12 s: 5 embryos, 156 cells ; 14 s: 9 embryos, 208 cells ; 16 s,: 9 embryos, 220 cells ; 18 s: 5 embryos, 143 cells ; 26 s: 4 embryos, 119 cells). **c-f)** Live imaging of BB movements during the polarization process. Images were taken every 5 minutes; a selection of images is presented here from two early stage embryos (**c, d** movies between the 6 s and 9 s stages; **d** yellow arrow points at an anterior contact event) and two late stage embryos (**e, f.** movies between the 18 s and 21 s stages). The distances between BBs and posterior membranes were then plotted (green curve, “a” in the scheme in Fig1b) along with the distance between the anterior and posterior membranes (magenta curve, “b” in the scheme in Fig1b) and the p.i. (dashed blue curve). Black arrows on the graphs indicate the position of the images displayed on the left. **g)** Quantification of the percentage of total movie time spent by the BB in contact with the posterior membrane. (4-8s: 5 embryos, 41 cells; 13-17s: 6 embryos, 38 cells; 17-21s: 7 embryos, 59 cells). **h, i)** Number of contact events per h between BB and anterior membrane (**h**) or between BB and posterior membrane (**i**) in embryos filmed at different developmental stages: 4 to 8 s (5 embryos, 41 cells), 13

to 17 s (5 embryos, 25 cells) and 17 to 21 s (7 embryos, 32 cells). Cells with a BB in contact with the posterior membrane during the whole movie (points at 100% in Fig1g) were not plotted here. Statistical significance was assessed using a Wilcoxon test. *Scale bars:* 2 *µ*m.

Figure 2. Par3 forms patches and is asymmetrically localized in FP cells.

a, b) Individual cells from dorsal views of 14 s stage embryos showing IF with a Par3 antibody (a) or an antibody recognizing a phosphorylated form of Par3, BazP1085 (b) in FP cells. Two distinct cells are shown for each antibody. Both total Par3 and its phosphorylated form localize at apical junctions and are enriched at tricellular junctions (yellow arrowhead in a) and in patches at transverse membranes (white arrows), whether the BB is in contact with the posterior membrane (left images) or not (right). **c)** Representative images of isolated FP cells expressing Par3-RFP and Centrin-GFP at early (8 s, left) or late (17 s, right) stages. **d)** Par3-RFP posterior/anterior fluorescence intensity ratio in fully polarized FP cells (such as those displayed in **c**) at early and late stages. The red dotted line indicates a ratio of 1 (corresponding to a symmetric Par3-RFP distribution) (comparison was done using a Wilcoxon test). **e-g)** Images of time-lapse movies showing individual FP cells from embryos mosaically expressing Par3-RFP (magenta) and centrin-GFP (green) (lateral view). Par3-RFP posterior/anterior fluorescence intensity ratio is plotted on the right plots (magenta curve) along with the polarization index (« p.i. », dashed blue curve). Black arrows on plots indicate the time-points corresponding to the images displayed on the left. **e)** FP cell with Par3 posterior enrichment in an embryo filmed between the 15 s and 17 s stages. Par3 posterior enrichment starts 20 min after the beginning of the movie (magenta arrow), 10 min before BB/posterior membrane contact (green arrow). **f)** FP cell with Par3 posterior enrichment in an embryo filmed between the 8 s and 10 s stages. Par3 posterior enrichment starts 20 min after the beginning of the movie (magenta arrow), 20 min before BB/posterior membrane contact (green arrow). **g)** FP cell with no posterior Par3 enrichment (Par3-RFP post/ant ratio close to 1) with a BB oscillating around the middle of the apical surface, in an embryo filmed between 17 s and 19 s. Scale bars : 2*µ*m.

Figure 3. BB/Par3 patches exclusive contacts at early stages and Par3 over-expression

a-c) Images from time lapse movies of embryos mosaically injected with centrin-GFP (green), Membrane-GFP (green) and Par3-RFP (magenta) mRNAs. All pictures are dorsal views of FP cells. **a)** global view of 6 adjacent FP cells at the beginning of the movie shown in **b** ; white arrows point at Par3 patches (aligned along the AP axis) with which BB make contacts during the movie. The dotted frame indicates the position of the cell whose behavior is shown in **b**. **b)** example of a FP cell between the 4 and 5s stages, whose BB is in contact with the anterior Par3 patch at the beginning of the movie but then makes contact with the posterior Par3 patch that stretches in its direction (yellow arrows). A close up of BB and Par3 patches is shown for t=30'. **c)** Example of posterior and anterior membrane invaginations originating from Par3 patches and partially coated with Par3. Yellow arrows point to posterior (t=0') and anterior (t=64') invaginations. White arrowheads point to Par3 patches. Par3 patch deformation is more obvious at t=64' but is also present at t=0'. A close up of BB, Par3 patches and posterior membrane invagination is shown for t=0'. **d)** Polarization index (p.i., cf Fig1) of FP cells from embryos mosaically over-expressing either MbCherry (control) or Par3-RFP. We quantified both the polarization index of MbCherry or Par3-RFP positive cells and the polarization index of MbCherry or Par3-RFP negative cells. Scale bar : 2μm. Comparison was done using a Wilcoxon test.

Fig. 4 Par3 clustering and localization in *vangl2*^{m209} mutant FP

a) Polarization index of *vangl2*$^{m209/m209}$ determined from immunostaining data (wt: 2 embryos, 49 cells; *vangl2*$^{m209/+}$ 3 embryos, 66 cells; *vangl2*$^{m209/m209}$ 5 embryos, 57 cells) **b)** Immunostaining of phoshorylated Par3 (BazP1085 antibody) in *vangl2*$^{+/+}$ (wt) and *vangl2*$^{m209/m209}$ mutant embryo FP at 18 s. In each case ZO1 staining was removed in the right image to reveal Par3 patches (yellow arrows). **c)** Quantification of the number of Par3 patches per cell on transverse membranes from immunostaining data as shown in b. **d)** The same method as in c. was used to extract phospho-Par3 patches prominence, defined as the height of Par3 fluorescence peak relative to the highest and nearest valley (local fluorescence

minimum) (for each cell, prominence is normalized by the lowest Par3 intensity value). Right scheme: yellow arrows: tricellular junctions; white bar: orientation of the fluorescence measurement along the transverse membrane, star: position of Par3 patch. In a-d, *vangl2*$^{+/+}$: N=7, n=186 ; *vangl2*$^{m209/+}$: N=5, n=112 ; *vangl2*$^{m209/m209}$: N=7, n=129. **e, f)** Images from movies of 5s *vangl2*$^{m209/m209}$ embryos mosaically injected with Par3-RFP, Centrin-GFP and Membrane-GFP mRNA at the 16-32 cell stage. Yellow arrows point at contact events between Par3 patches and BBs. **g)** Percentage of cells displaying a lateral Par3-RFP patch in live-imaging experiments such as the one described in e,f. (*vangl2*$^{+/+}$ and *vangl2*$^{m209/+}$: N=16, n=45 ; *vangl2*$^{m209/m209}$: N=7, n=17). Statistical tests: Wilcoxon test for comparison of p.i. and prominence; Fisher test for comparison of patch number and percentage of cells with lateral patches.

SUPPLEMENTARY FIGURE LEGENDS

Supplementary Figure S1: Further characterization of FP polarization in space and time.

a Quantification of FP polarization along the AP axis at 12 s. Analysis was performed on fixed immunostained embryos as described in Fig1a. (Wilcoxon test p-values for successive AP axis levels are: 0.6095, 0.5514, 0.3596, 0.3668, 0.5487, N=5, n=156 the difference between first and last AP axis levels were also small and non-statistically significant). **b** Still images from FP BB (green) and membrane (magenta) live imaging (dorsal view, start at 14s stage). The yellow arrow points to BB that will move and make contacts with the posterior membrane between 0 and 50 min after the movie started. White arrowheads point at BBs in adjacent cells that stay in contact with the posterior membrane during this time interval. **c** BB speed measured from live-imaging data at different developmental stages. The speed of each BB movement was calculated by dividing the value of BB/posterior membrane variations (corresponding to green curves in Fig1 c-f) by the total duration of the movement (4-8s: 4 embryos, 38 cells; 13-17s: 6 embryos, 22 cells; 17-21s: 7 embryos, 32 cells). Comparison between stages was done using a Wilcoxon test. **d** Still images from a movie of a 5 s to 7 s stage embryo injected with centrin-GFP (green) and MbCherry (magenta) showing a dividing FP cell. Yellow arrows point at the BB of the anterior daughter cell, which rapidly moves back to the posterior membrane after cytokinesis. **e** Movies described in Fig1 were used to quantify BB direction change frequency, mean duration of BB/posterior membrane contact events as a percentage of total imaging duration and mean polarization index during live-imaging. Plots in the first line take into account the BBs that stay in contact with the posterior membrane 100% of movie duration (posteriorly docked BBs) whereas the second line only represents BBs that are not posteriorly docked. Comparison between stages was done using a Wilcoxon test. Scale bar : 2μm.

Supplementary Figure S2: Membrane invaginations link BBs to transverse membranes during FP polarization

a, b) Left : images taken from live-imaging data such as those presented in Fig. 1. Yellow arrows : potential cilia. Time (in minutes) is indicated in the upper-left corner. Right : count of transverse membrane invagination events in FP cells at early (before 14s) and late stages (after14s). a shows a posterior membrane invagination (white arrows); b shows an anterior membrane invagination (white arrow). Short mbCherry-positive digitations, presumably corresponding to cilia, were in some cases associated to the BB opposite the invagination (yellow arrowheads in a and b). These membrane digitations were rare in late stage embryos (6/57 cells out of 10 embryos) compared to early embryos (44/68 cells from 9 embryos), suggesting that Mb-Cherry entry into cilia is less common at later stages, which could reflect a maturation of the ciliary gate. **c)** Number of timepoints where anterior or posterior invaginations were detected in time-lapse movies with a 5 minutes interval between images (10 embryos, 24 cells, Wilcoxon test) d) Behavior of BB immediately after formation of an anterior or posterior invagination: BB either moved anteriorly ('ant'), posteriorly ('post') or did not move ('immobile') (50 posterior and 14 anterior invaginations from 16 embryos, 35 cells, Fisher test).

Supplementary Figure S3: *Par3ab* morphants or mutants have normal FP polarization and Par3 patches

a) FP polarization index (p.i.) in non-injected (NI) and Par3ab morpholino (MO)-injected embryos at 18s stage (NI : N=9, n=171 ; Par3MO : N=16, n=244). **b)** BazP1085 patch prominence (left) and number (right) in NI and Par3ab MO injected embryos at 18s stage (NI : N=4, n=66 ; Par3MO : N=3, n=38). **c)** p.i. of maternal zygotic heterozygous (*MZPar3ab*$^{+/-}$) or homozygous (*MZPar3ab*$^{-/-}$) Par3ab mutants at 18s stage (*MZPar3ab*$^{+/-}$: N=7, n=106 ; *MZPar3ab*$^{-/-}$: N=9, n=152). **d)** Par3 patches prominence (left) and number (right) in maternal zygotic heterozygous (*MZPar3ab*$^{+/-}$) or homozygous (*MZPar3ab*$^{-/-}$) Par3ab mutants at 18s stage (*MZPar3ab*$^{+/-}$: N=3, n=27 ; *MZPar3ab*$^{-/-}$: N=3, n=59). **e)** Immunostaining of FP cells over-expressing Par3-RFP in embryos mosaically injected with Par3-RFP mRNA at the 16 cells stage (dorsal view, 18 s stage). Par3 or BazP1085 patches number compared with Fisher's exact test. **f)** Immunostaining of FP cells not injected (NI) or injected with Par3ab

morpholino (Par3abMO) showing the equivalent amount of BazP1085 staining in both conditions. **g)** Immunostaining of FP cells in MZPar3ab$^{+/-}$ and MZPar3ab$^{-/-}$ showing the equivalent amount of Par3 in both genotypes.

SUPPLEMENTARY MOVIES LEGENDS

Filename: Supplementary movie 1
Description: **Live imaging of a BB bouncing off the posterior membrane in an early-stage FP cell**. wt embryos were injected with Centrin-GFP (green) and membrane-Cherry (magenta) mRNAs at the one-cell stage. White arrows indicate the position of the BB at the first and last time-points. Images were taken every 5 minutes during the 6 s to 9 s stages time-frame. Dorsal view. Corresponds to Fig1c.

Filename: Supplementary movie 2
Description: **Live imaging of a BB bouncing off posterior and anterior membranes in an early-stage FP cell**. wt embryos were injected with Centrin-GFP (green) and membrane-Cherry (magenta) mRNAs at the one-cell stage. White arrows indicate the position of the BB at the first and last time-points. Images were taken every 5 minutes during the 6 s to 9 s stages time-frame. Dorsal view. Corresponds to Fig1d.

Filename: Supplementary movie 3
Description: **Live imaging of a BB staying in contact with the posterior membrane in a late-stage FP cell**. wt embryos were injected with Centrin-GFP (green) and membrane-Cherry (magenta) mRNAs at the one-cell stage. White arrows indicate the position of the BB at the first and last time-points. Images were taken every 5 minutes during the 18 s to 21 s stages time-frame. Dorsal view. Corresponds to Fig1e.

Filename: Supplementary movie 4
Description: **Live imaging of BB bouncing against the posterior membrane in a late-stage FP cell**. wt embryos were injected with Centrin-GFP (green) and membrane-Cherry (magenta) mRNAs at the one-cell stage White arrows indicate the position of the BB at the first and last time-points. Images were taken every 5 minutes during the 18 s to 21 s stages time-frame. Dorsal view. Corresponds to Fig1f.

Filename: Supplementary movie 5
Description: **Live imaging of** the **rapid repolarization of the anterior daughter cell after FP cell division**. wt embryos were injected with Centrin-GFP (green) and membrane-Cherry (magenta) mRNAs at the one-cell stage. White arrows

(at the beginning, middle and end of the movie) point at the BB of the anterior daughter cell, which rapidly moves back to the posterior membrane after cytokinesis. Images were taken every 2 minutes during the 5 s to 7 s stages time-frame. Dorsal view. Corresponds to FigS1d.

Filename: Supplementary movie 6
Description: **Live imaging of BB movements in a FP cell displaying a membrane invagination between BB and the posterior membrane** (yellow arrow at t=115 min). wt embryos were injected with Centrin-GFP (green) and membrane-Cherry (magenta) mRNAs at the one-cell stage. White arrows point at the BB. Images were taken every 5 minutes during the 6 s to 9 s stages time-frame. Dorsal view. Corresponds to FigS2a.

Filename: Supplementary movie 7
Description: **Live imaging of BB movements in a FP cell displaying a membrane invagination between BB and the anterior membrane** (yellow arrow at t=18 min). wt embryos were injected with Centrin-GFP (green) and membrane-Cherry (magenta) mRNAs at the one-cell stage. Membrane invaginations between the posterior membrane and BB can also be seen at t=10min, t=26min and t=66min. White arrows point at the BB. Images were taken every 2 minutes during the 8 s to 10 s stages time-frame. Dorsal view. Corresponds to FigS2b.

Filename: Supplementary movie 8
Description: **Live imaging of BB movements and Par3-RFP localization in a polarizing FP cell**. wt embryos mosaically expressing Centrin-GFP (green) and Par3-RFP (magenta). White arrows point at the BB at t=0 and at t=30 min, when the BB touches the posterior membrane. Images were taken every 2 min during the 15 s to 17 s stages time-frame. Lateral view. Corresponds to Fig2e.

Filename: Supplementary movie 9
Description: **Live imaging of BB movements and Par3-RFP localization in a polarizing FP cell**. wt embryos mosaically expressing Centrin-GFP (green) and Par3-RFP (magenta). White arrows point at the BB at t=0 and at t=60 min, when the BB touches the posterior membrane. Images were taken every 4 min during the 8 s to 10 s stages time-frame. Dorsal view. Corresponds to Fig2f.

Filename: Supplementary movie 10
Description: **Live imaging of BB movements and Par3-RFP localization in a non-polarizing FP cell**. wt embryos mosaically expressing Centrin-GFP (green) and Par3-RFP (magenta). White arrows point at the BB at the beginning and end of movie. Images were taken every 5 minutes during the 17 s to 19 s stages time-frame. Lateral view. Corresponds to Fig2f.

Filename: Supplementary movie 11
Description: **Live imaging of BB/Par3 patch contacts in an early-stage FP cell**. wt embryo mosaically expressing Centrin-GFP, Membrane-GFP (green) and

Par3-RFP (magenta). White arrows point at the BB at the beginning of the movie, when the BB is in contact with the anterior Par3 patch, at t=30 min when it makes a contact with the posterior Par3 patch and at the end of the movie. Images were taken every 2 min during the 4 s to 5 s stages time-frame. Dorsal view. Corresponds to Fig3b.

Filename: Supplementary movie 12
Description: **Live imaging of membrane invaginations at the level of Par3 patches in early stage FP cells**. wt embryo mosaically expressing Centrin-GFP, Membrane-GFP (green) and Par3-RFP (magenta). White arrows point at the BB at the beginning and at the end of the movie. Yellow arrows at t=0 and t=68 min point at membrane invaginations originating from the posterior and the anterior Par3 patches, respectively. Images were taken every 4 min during the 7 s to 8 s stages time-frame. Dorsal view. Corresponds to Fig3c.

Filename: Supplementary movie 13
Description: **Live imaging of BB/lateral Par3 patch contacts in an early-stage FP cell of a *vangl2*$^{m209/m209}$ mutant**. *vangl2*$^{m209/m209}$ embryo mosaically expressing Centrin-GFP, Membrane-GFP (green) and Par3-RFP (magenta). White arrows point at the BB at the beginning and at the end of the movie. Images were taken every 4 min during the 5 s to 6 s stages time-frame. Dorsal view. Corresponds to Fig4e.

Filename: Supplementary movie 14
Description: **Live imaging of BB/posterior Par3 patch contacts in an early-stage FP cell of a *vangl2*$^{m209/m209}$ mutant**. *vangl2*$^{m209/m209}$ embryo mosaically expressing Centrin-GFP, Membrane-GFP (green) and Par3-RFP (magenta). White arrows point at the BB at the beginning and at the end of the movie. Images were taken every 4 min during the 5 s to 6 s stages time-frame. Dorsal view. Corresponds to Fig4f.

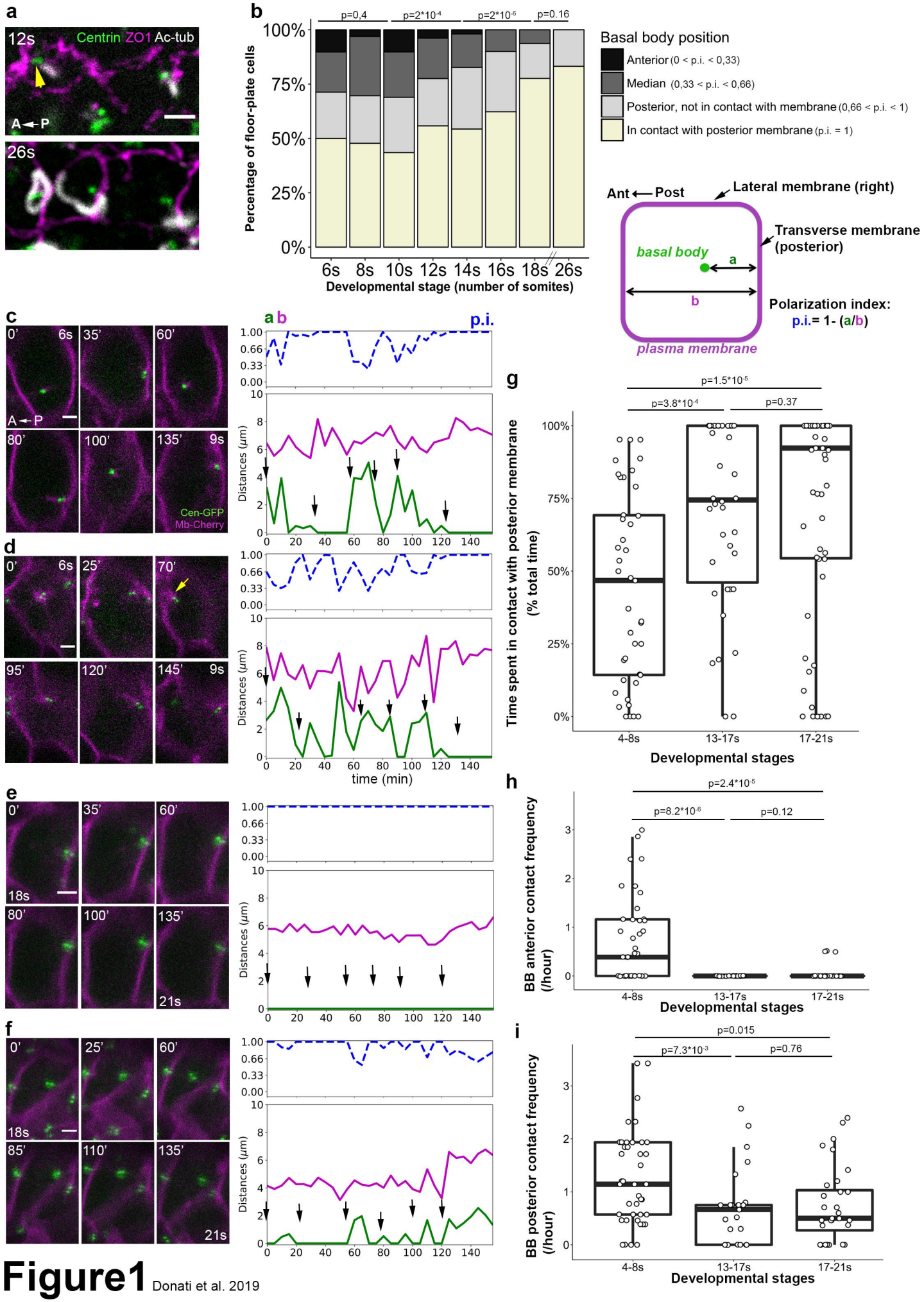

Figure1 Donati et al. 2019

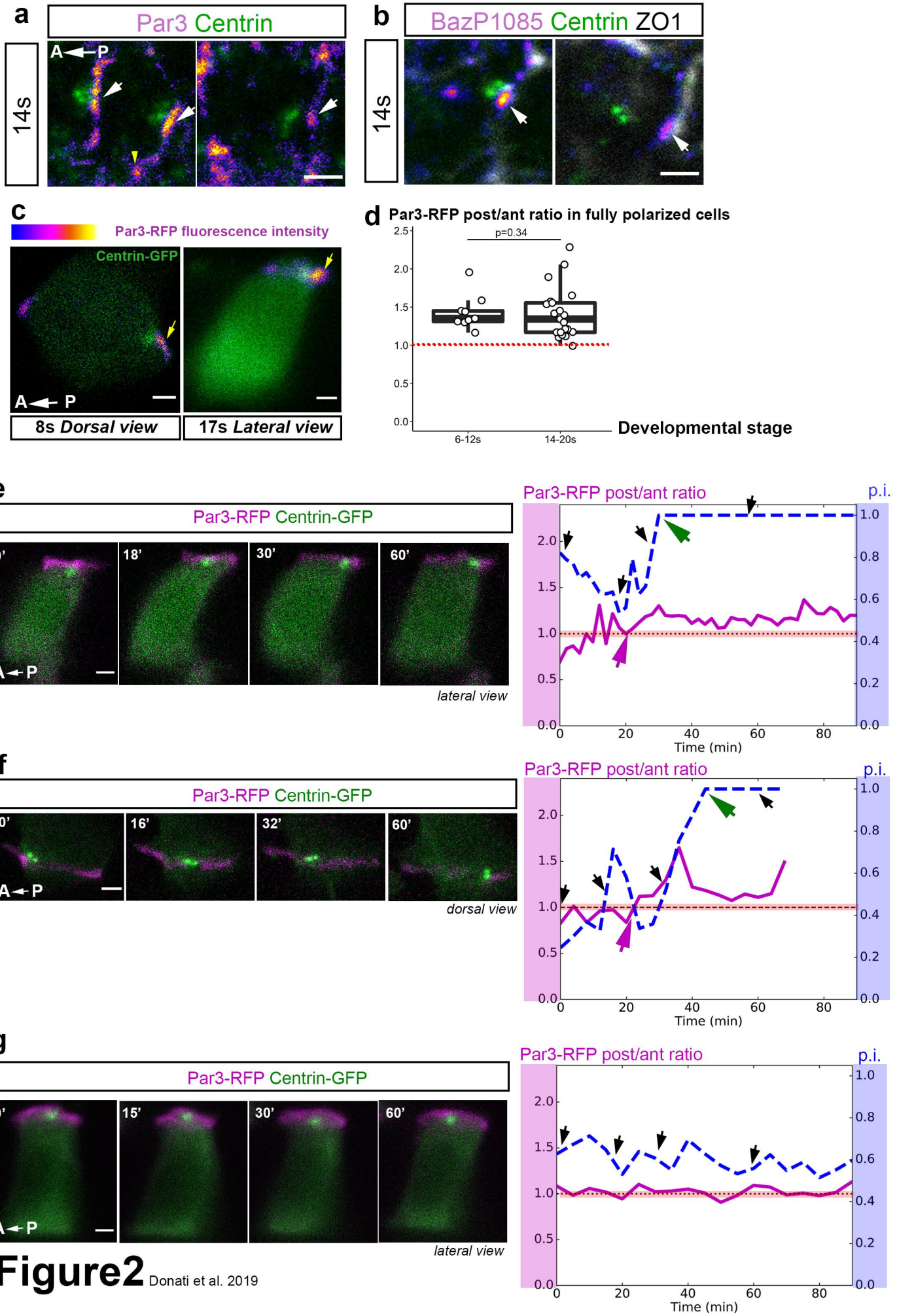

Figure2 Donati et al. 2019

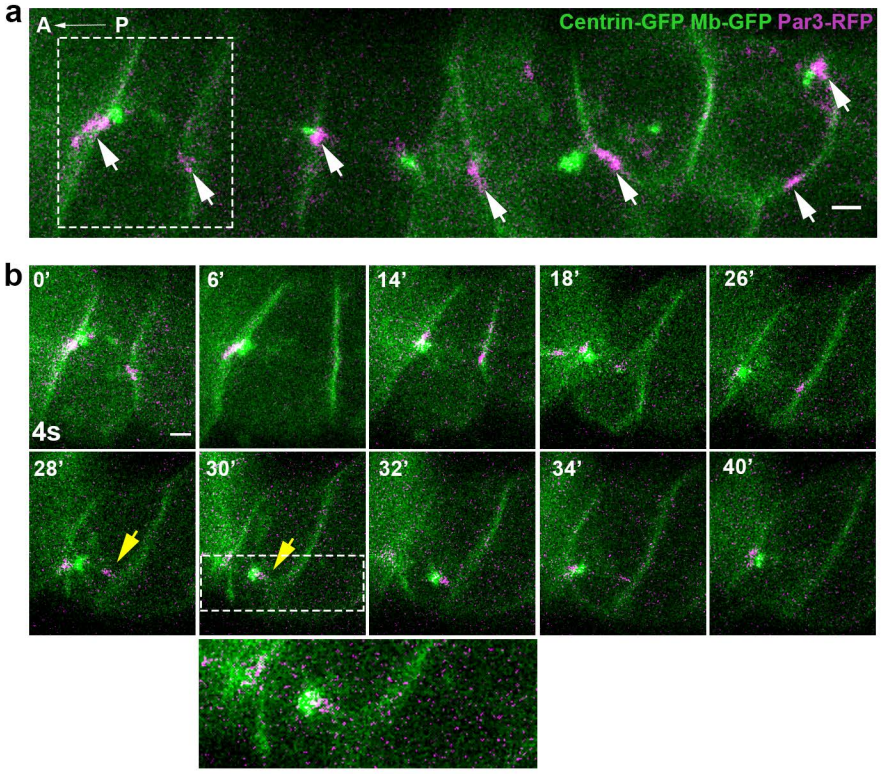

Figure3 Donati et al. 2019

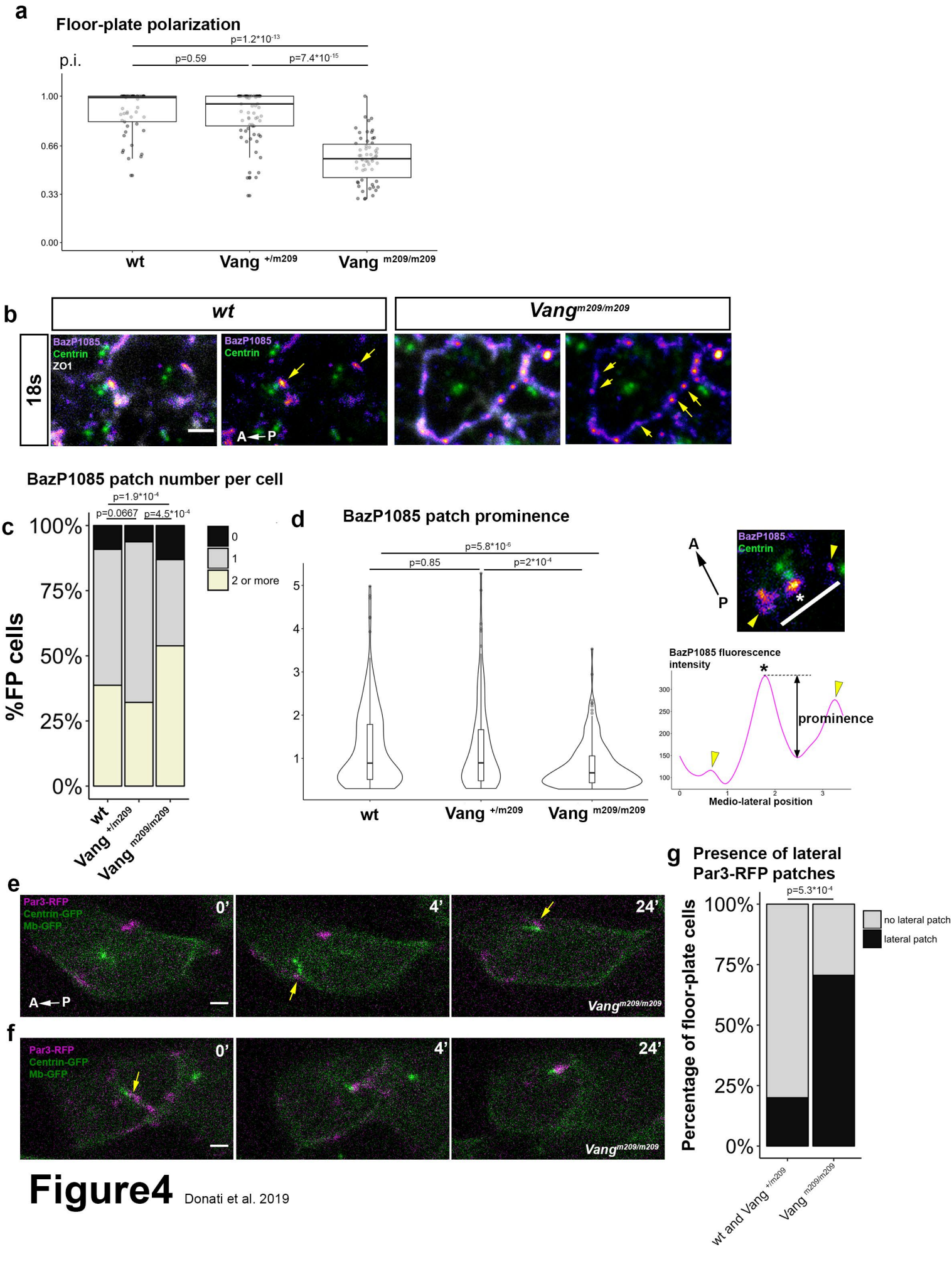

Figure4 Donati et al. 2019

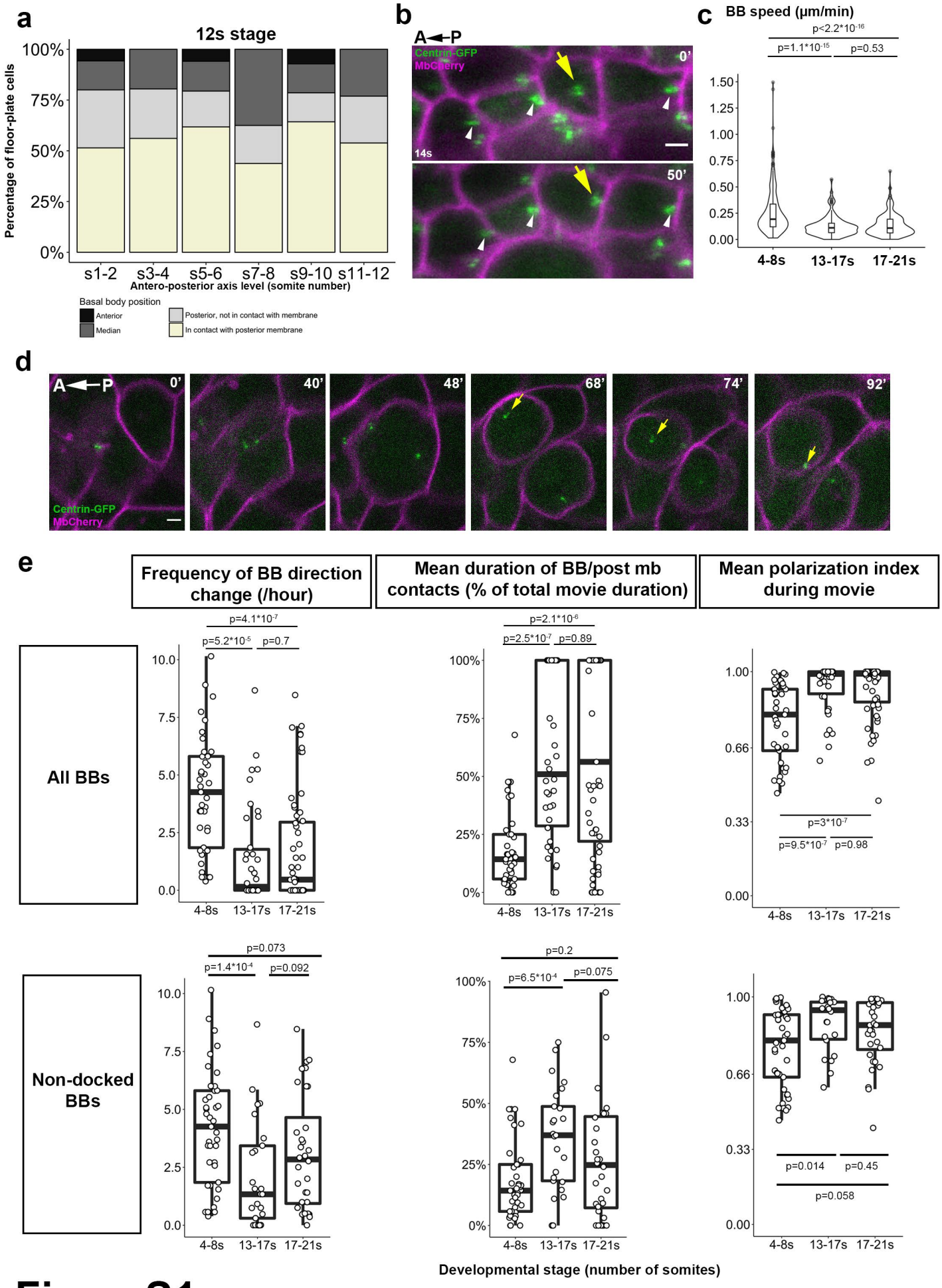

FigureS1 Donati et al. 2019

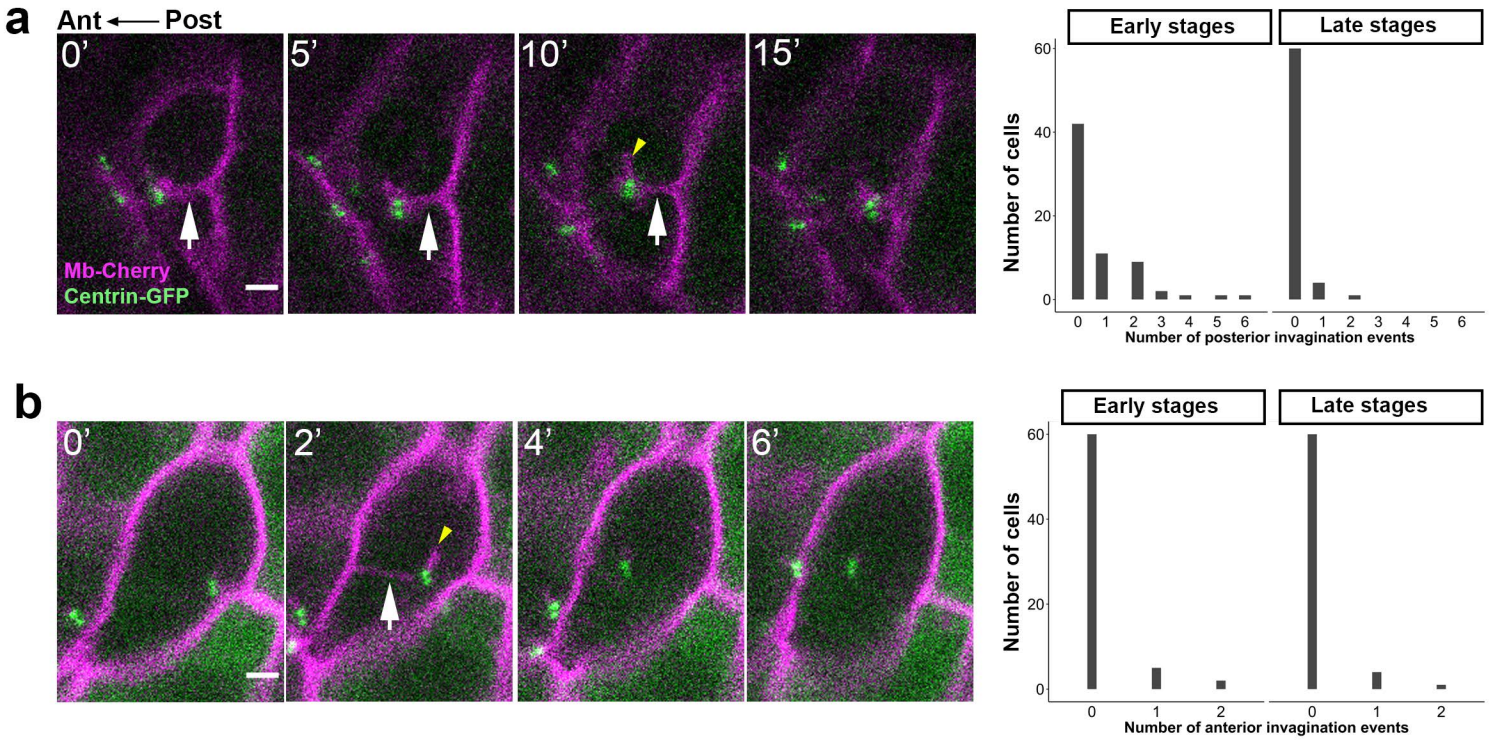

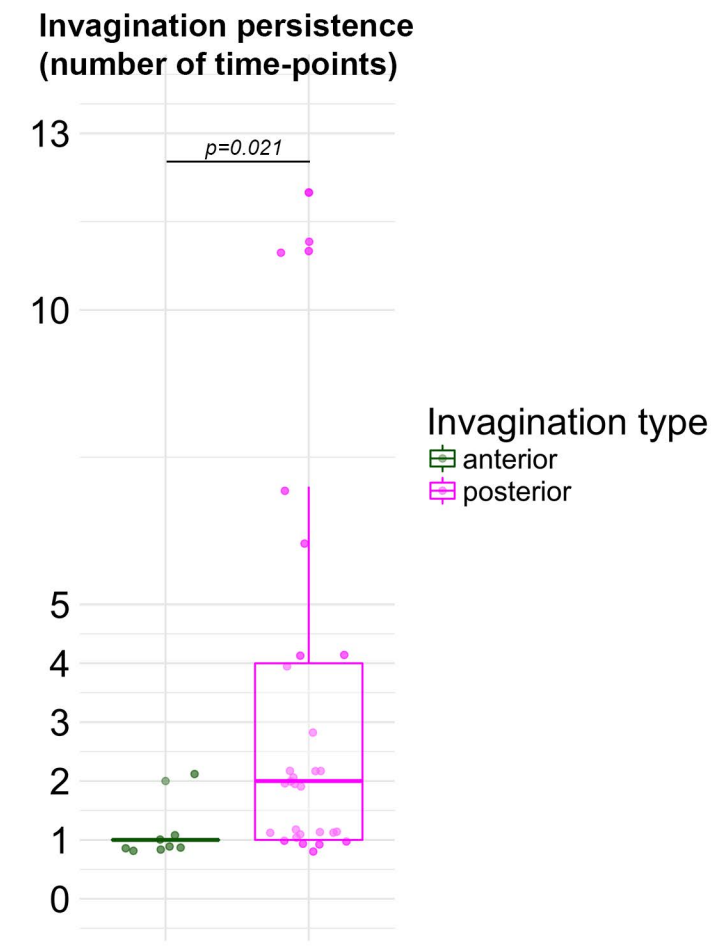

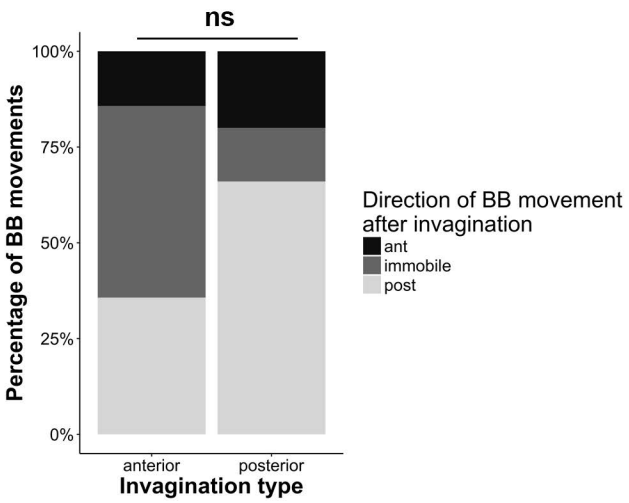

FigureS2 Donati et al. 2019

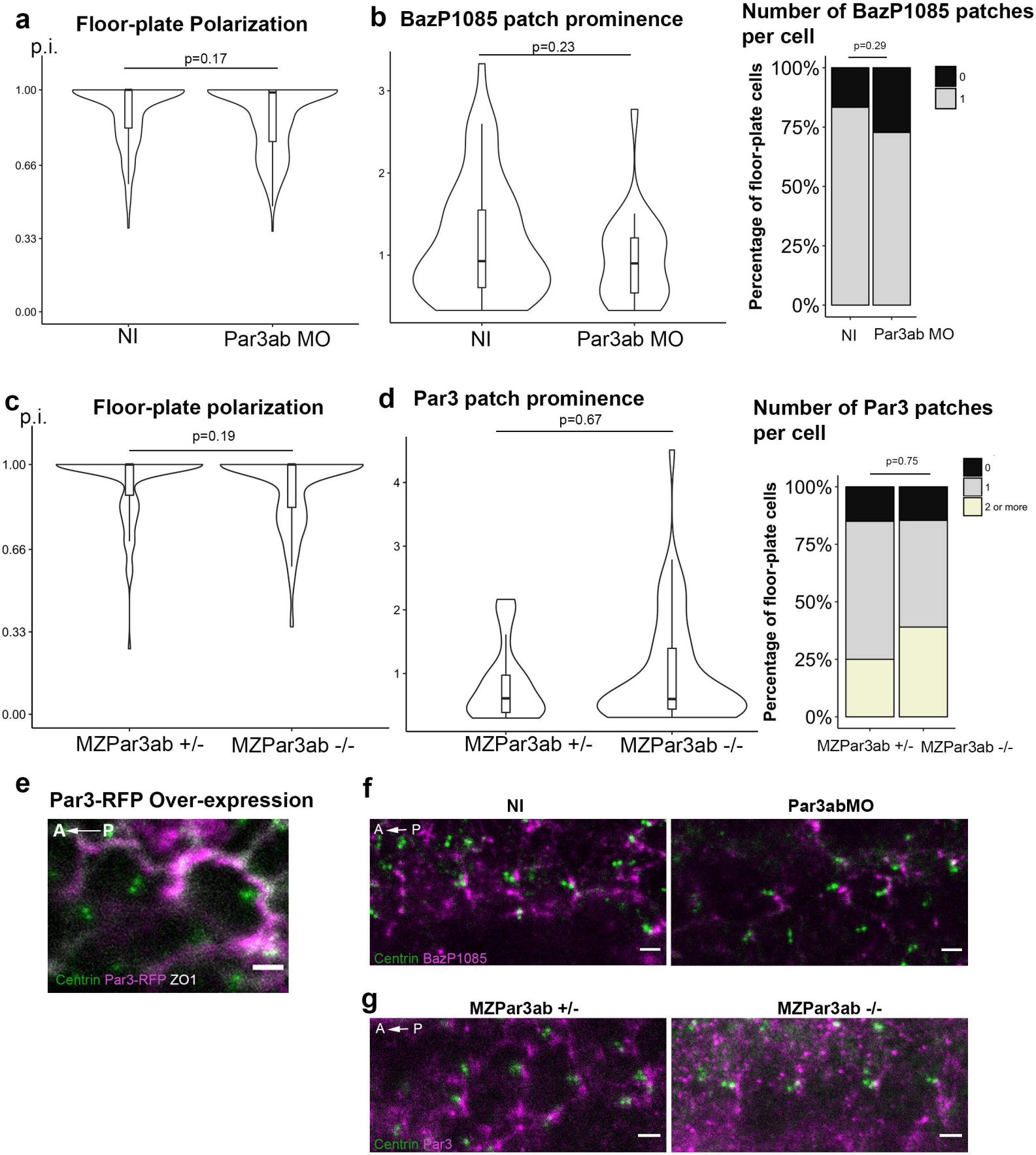

Figure S3 Donati et al.2019